Available online at www.sciencedirect.com

SciVerse ScienceDirect

Journal of the European Ceramic Society 32 (2012) 875–882

www.elsevier.com/locate/jeurceramsoc

The influence of processing on the microstructure and the microwave properties of Co–F-codoped barium strontium titanate thick-films

A. Friederich [a,*], X. Zhou [a,b], M. Sazegar [b], J. Haußelt [a], R. Jakoby [b], M.J. Hoffmann [c], J.R. Binder [a]

[a] *Institute for Applied Materials (IAM-WPT), Karlsruhe Institute of Technology, Hermann-von-Helmholtz-Platz 1, 76344 Eggenstein-Leopoldshafen, Germany*
[b] *Institute for Microwave Engineering and Photonics (IMP), Technische Universität Darmstadt, Merckstraße 25, 64283 Darmstadt, Germany*
[c] *Institute for Applied Materials (IAM-KM), Karlsruhe Institute of Technology, Haid-Und-Neu-Str. 7, 76131 Karlsruhe, Germany*

Received 31 August 2011; received in revised form 2 November 2011; accepted 3 November 2011
Available online 1 December 2011

Abstract

The influence of processing on the microstructure and the dielectric properties of Co–F-codoped $Ba_{0.6}Sr_{0.4}TiO_3$ (BST) thick-films has been investigated. BST powders with different particle sizes were prepared and applied on alumina substrates by screen-printing. The resulting thick-films were sintered at different holding times and characterized with respect to their microstructure and microwave properties. The microstructure of the thick-films shows a clear dependency on sintering time and initial particle size. In addition to grain growth, the formation of a secondary phase is observed at the interface between substrate and BST with increasing sintering time. The dielectric characterization at microwave frequencies shows an increase of tunability with larger grain size while the dielectric loss is even lowered. This shows the strong influence of the microstructure on the material properties and the possibility of tailoring the material through specific processing.

Keywords: BST; Thick-film; Grain size; Porosity; Microwave properties

1. Introduction

Ferroelectric ceramics are promising candidates for passive tunable devices such as phase shifters, tunable matching networks, tunable filters and tunable antennas.[1–3] Currently most attention is given to the solid solution $Ba_xSr_{1-x}TiO_3$ (BST). This is due to the fact that the material shows low dielectric loss and a considerable field dependency of permittivity (i.e. tunability). In addition, the Curie temperature can be easily adapted to the application environment by changing the Ba to Sr ratio.

It is well documented that acceptor doping of the perovskite can be used to remarkably reduce the dielectric loss of BST at high frequencies.[4–8] However, this usually comes with a reduction of the material's tunability. Previous investigations showed that metal–fluorine-codoping of BST can lead to a decrease of the dielectric loss while holding the tunability on a level comparable to that of undoped BST thick-films.[9,10] The influence of acceptor–donor-doping of BST with metal and fluorine is not completely understood yet. While the codoping shows a significant influence on the properties of the material, the incorporation of fluorine has not yet been proved directly.[9,10]

Several metal elements act as acceptor dopants in BST when occupying the A- or B-site of the perovskite and having a lower oxidation state compared to the substituted ion. It is reported that Co is incorporated at the B-site of the perovskite structure with a oxidation state +3 under oxygen- or oxygen–nitrogen-atmosphere in $BaTiO_3$.[11,12] Assuming that this also holds for BST, a Co-doping leads to one oxygen vacancy per two incorporated Co-atoms in the perovskite structure. It is assumed that the fluorine occupies the oxygen vacancies caused by the acceptor-doping and thereby reduces the dielectric loss mechanisms. As doping not only affects the defect chemistry of the material but also its sintering behaviour, changes in the dielectric properties have to be considered with regard to the present microstructure.

It is obvious that the effective permittivity of a ferroelectric thick-film is decreased with increasing porosity. For grain sizes below 0.7 μm, $BaTiO_3$ shows a reduction of permittivity and a less discrete phase transition with decreasing grain size.[13,14] For $Ba_xSr_{1-x}TiO_3$ ($x = 0.3, 0.5, 0.7$) similar results are reported for a frequency of $f = 100$ kHz.[15,16] So far, there are only few

* Corresponding author. Tel.: +49 721 608 24056; fax: +49 721 608 24612.
E-mail address: andreas.friederich@kit.edu (A. Friederich).

0955-2219/$ – see front matter © 2011 Elsevier Ltd. All rights reserved.
doi:10.1016/j.jeurceramsoc.2011.11.010

reports about microstructural influences on the dielectric properties of BST thick-films for frequencies above 1 GHz. It was shown experimentally and confirmed by simulation that permittivity as well as tunability of undoped $Ba_{0.6}Sr_{0.4}TiO_3$ could be increased slightly by shifting the median grain diameter from 0.34 to 0.38 μm.[17]

This article deals with the effect of grain size and porosity on tunability, dielectric loss and permittivity of screen-printed $Ba_{0.6}Sr_{0.4}TiO_3$ thick-films at microwave frequencies. The powder preparation process and the sintering of the thick-films were varied to achieve a larger range of grain sizes and different porosities. For the investigations a Co–F-codoping of the BST was chosen since previous investigations showed the lowest dielectric loss at lower GHz-frequencies for this composition when compared to other metal-fluorine codoped and undoped BST thick-films.[10]

2. Experimental

Co–F-codoped barium strontium titanate powders were synthesized through a modified sol–gel process. The nominal stoichiometric composition was chosen to $Ba_{0.6}Sr_{0.4}Ti_{0.99}Co_{0.01}O_{3-x}F_{0.09}$, where x ensures electric neutrality depending on the undetermined oxidation state of the components.

For the synthesis barium acetate (0.42 mol), strontium acetate hemihydrate (0.28 mol) and trifluoracetetic acid (21.0 mmol) were dissolved in acetetic acid (29.9 mol) and stirred over night in a chemical reactor under nitrogen atmosphere. Titanium-(IV)-isopropoxide (0.70 mol) was added and a clear sol formed. Cobalt acetate tetrahydrate (7.0 mmol) was dissolved in water (181.3 mol, specific conductance $\sigma < 10^{-9}$ S/m) and added to the reactor. The diluted sol was filtered (mesh width: 1 μm) and spray-dried. The obtained metal–organic precursor was calcinated in alumina crucibles in a tube furnace at 900 °C for 1 h.

One part of the powder was milled using an attritor, a second and a third part using a planetary ball mill. The milled powders were dispersed in terpineol using a dispersant (Hypermer KD1) and a binder (ethyl cellulose) to obtain suitable screen-printing pastes. One paste was created using the attriton-milled powder. A second and a third paste were created using the planetary-ball-milled powder and a mixture of both types of powders, respectively. In the latter case, a ratio of 30:70 was chosen for the proportion of attriton-milled powder to planetary-ball-milled one. The pastes were dispersed in two steps by using a dissolver and a three roll mill for each paste. All pastes were printed on polycrystalline alumina substrates (Rubalit® 710, CeramTec). After drying at 50 °C for 24 h the specimen were cold isostatically densified at 400 MPa for 3 min to avoid cracking during sintering. Eventually the thick-films were sintered at 1200 °C for 1 h, 10 h and 24 h, respectively. The thermal treatment in the tube furnace (calcination and sintering) was done under dried purified air (molecular sieve and silica gel) with heating rates and cooling rates of 5 K/min. A schematic plan of powder, paste and thick-film preparation is shown in Fig. 1.

The stoichiometry of the metal elements in the powders was measured using X-ray fluorescence spectroscopy (SRS 303AS, Bruker-AXS). Titration after pyrohydrolysis (at the laboratory of H.C. Starck GmbH, Goslar, Germany) was used to determine the amount of fluorine present in the powders. Additionally small amounts of screen-printing pastes were calcinated under sintering conditions and analyzed in regard to their fluorine content, too.

The specific surface area of the powders was determined by single point BET measurement (FlowSorb II 2300, Micromeritics). Assuming homogeneous monodisperse spherical particles with neglectable contact area, the BET diameter d_{BET} was calculated and used as an estimation for the primary particle size of the powders. With the measured specific surface area A_{BET} and the theoretical density ρ it can be calculated after

$$d_{BET} = \frac{6}{\rho A_{BET}}. \quad (1)$$

The size of primary particles and aggregates was determined by laser diffraction (Horiba LA950, Retsch Technology) in isopropyl alcohol ($n_{IPA} = 1.378$),[18] assuming the complex refractive index of BST: $n_{BST} = 2.4 - 0.1i$.

The phase content of powders and sintered thick-films was examined by X-ray diffraction (D5000, Siemens, Cu-radiation: $K_{\alpha 1}$ and $K_{\alpha 2}$). Scanning electron microscopy (Supra 55, Zeiss) was used to investigate the microstructure of the powders and the thick-films. Grain size distribution and thick-film height were determined by image analysis (analySIS pro, Olympus Soft Imaging Solutions) of several SEM pictures. The porosity P was calculated through the measured height h and weight m of the thick-films, the lateral dimensions of the print layout (square, $x = 47.5$ mm) and the theoretical density after

$$P = 1 - \frac{m}{\rho h x^2}. \quad (2)$$

The microwave properties of the thick-films were determined by measuring the scattering parameters (S-parameters) of coplanar waveguides (CPW) applied on the top surface of the sintered films. On each specimen multiple waveguides were realized through a lithography step on a evaporated Cr/Au seed layer followed by a galvanic growth of Au. After the galvanization to a thickness of at least 1.5 μm the photoresist and the remaining seed layer were removed through etching. The S-parameters were determined by temperature controlled ($T = 23$ °C) on-wafer measurements using a vector network analyzer in a frequency range of 0.1–40 GHz at tuning voltages U between 0 and 100 V (step size 10 V). The bias field E was calculated with tuning voltage and gap width s of the CPWs after $E = U/s$.

The relative effective permittivity $\varepsilon_{r,eff}$ and dissipation factor $\tan\delta$ of the thick-films were extracted from the measured S-parameters by conformal mapping model based method. This method allows the extraction of the values for each measuring point taking into account the geometry and the properties of the substrate and the waveguides.[19,20] The CPW geometry used allows to extract reliable dielectric properties in the frequency range 5–40 GHz.

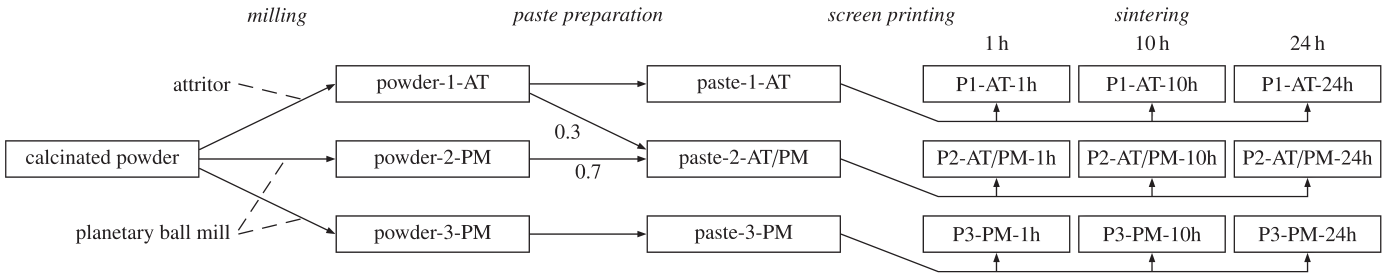

Fig. 1. Process plan for powder, paste and thick-film preparation. Milling of the calcinated powder was done with a attritor (· · ·-AT) and planetary ball mill (· · ·-PM), respectively. The ratio for the powder mixture was chosen to 0.3:0.7, the sintering times for each paste to 1, 10 and 24 h, respectively.

The relative permittivity of the material $\varepsilon_{r,BST}$ (without influence of porosity) was estimated after the spherical inclusion model[1] simplified for a large effective permittivity ($\varepsilon_{r,eff} \gg 1$) after

$$\varepsilon_{r,BST} = \left(1 - \frac{3P}{2}\right)^{-1} \varepsilon_{r,eff}. \quad (3)$$

Strictly speaking, this equation holds only for small porosities ($P \ll 1$) and separated spherical pores. Nevertheless, Wersing et al.[21] showed that it is a good approximation even for porosities up to $P \approx 0.5$. Eventually, the relative tunability τ of the thick-films was calculated with the extracted permittivity values after

$$\tau(E, f) = \frac{\varepsilon_{r,eff}(E = 0, f) - \varepsilon_{r,eff}(E, f)}{\varepsilon_{r,eff}(E = 0, f)}. \quad (4)$$

To compare different materials in terms of their tunable performance and, hence, their capability for microwave applications, the material's figure of merit η is used.[22] With the tunability τ and the dissipation factor $\tan\delta$ in tuned state it is calculated after

$$\eta(E, f) = \frac{\tau(E, f)}{\tan\delta(E, f)}. \quad (5)$$

All microwave properties given in this publication were determined by measuring at least 10 test structures for relative permittivity and dissipation factor and 3 test structures for tunability and material's figure of merit per sample.

3. Results and discussion

3.1. Characterization of powders and pastes

To verify the chemical composition, the powders were analyzed by X-ray fluorescence spectroscopy (XRF) and titration after pyrohydrolysis. Table 1 shows the results of the XRF analysis. The measurements confirm that the amount of metal elements in the calcinated powders is almost the intended one. However, all powders show a small excess of A-site elements (Ba and Sr) to the B-site elements (Ti and Co) of the doped perovskite whose origin remains undetermined.

The results of titration after pyrohydrolysis are shown in Fig. 2 and in Table 3. The analysis reveals that the amount of fluorine in the powders after calcination is about 34–42% below the nominal value of the synthesis. After sintering for 1 h the fluorine content of the pastes is approximately half the initial value.

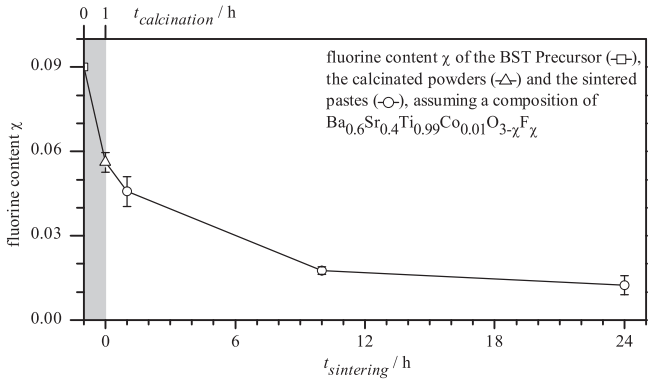

Fig. 2. Measured fluorine content of the calcinated powders and the pastes sintered at different holding times. The value given for the BST precursor is the initial amount for the synthesis. The gray area indicates the calcination at 900 °C whereas the white area represents the sintering process at 1200 °C.

For sintering times of 10 h and more the fluorine content drops to about 21% and less of the initial amount. Fig. 2 illustrates that the decrease of the fluorine content χ per time is lowered with higher sintering times and indicates that there might be a threshold value $\chi_t > 0$. This would support the assumption that flourine occupies the oxygen vacancies caused by acceptor-doping. This, however, does not explain where and how the remaining flourine is incorporated into the material for higher values. In addition there is no direct relation of the fluorine content to the particle and grain sizes of the powders and thick-films, which are presented below. In this publication the discussion of the microwave properties of thick-films sintered for 1 h is carried out neglecting the differences in fluorine content. This is based on the assumption that only a limited value of fluorine below the measured values is incorporated into the perovskite structure and the remaining amount is located at grain boundaries with a minor effect on

Table 1
Results of the XRF analysis of BST powders calcinated at 900 °C and milled by attritor (AT) and planetary ball mill (PM), respectively.

Sample name	Molar composition relative to BST			
	Ba[a]	Sr[a]	Ti[a]	Co[b]
Powder-1-AT	0.598	0.404	0.988	0.010
Powder-2-PM	0.600	0.405	0.984	0.010
Powder-3-PM	0.603	0.404	0.982	0.010

[a] Standard deviation $<1.5 \times 10^{-3}$.
[b] Standard deviation $<10^{-4}$.

Table 2
Results of BET surface measurements on the milled powders. d_{BET} represents a calculated diameter assuming monomodal spherical particles and a theoretical density of $\rho = 5.69$ g/cm^3.[10]

Sample name	A_{BET} (m^2/g)	d_{BET} (μm)[a]
Powder-1-AT	19.8	0.05
Powder-2-PM	7.3	0.14
Powder-3-PM	4.3	0.25

[a] Calculated according to Eq. (1).

the dielectric properties. The X-ray diffraction patterns shown in Fig. 3 reveal that the predominant phase of all powders is the cubic $Ba_{0.6}Sr_{0.4}TiO_3$ phase. Additionally, a small amount of $(Ba,Sr)F_2$ is formed, which is indicated by a weak reflex at $2\theta \approx 25°$ for the planetary ball milled powders. The formation of $(Ba,Sr)F_2$ is known from former investigations.[10] It is assumed that an excess of Ba and Sr in the composition supports the additional phase. This is in good agreement with the results from XRF analysis, where the planetary ball milled powders showed a larger ratio of A-site elements to B-site elements than the attriton milled one.

Compared to the planetary ball milled powders, the attriton-milled one shows broader reflexes. This indicates smaller crystallite sizes. To further investigate the primary particle size and to determine the agglomeration state of the powders, BET measurements and laser diffraction were carried out. Furthermore, SEM micrographs of the milled powders were taken and compared to the measurements.

Table 2 shows the results of the BET surface measurements. The specific surface of the attriton-milled powder is about 3–5 times larger than the planetary ball milled ones, which holds vice versa for the BET diameter. The micrographs of the powders shown in Fig. 4 support this result. In addition to the larger size of the primary particles in the planetary ball milled powders, powder-3-PM shows large aggregates, which states the smaller surface area of this powder. This could be led back to different conditions during the milling process, where the wet grinding time of powder-3-PM was shorter than for powder-2-PM due to a unintended evaporation of the liquid carrier (acetone). Laser diffraction showed that powder-3-PM has about

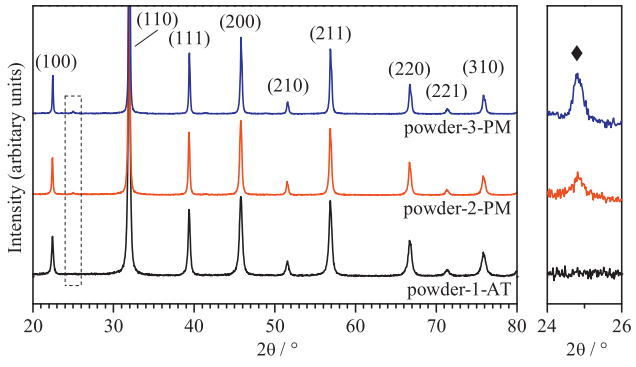

Fig. 3. X-ray diffraction patterns of powders calcinated at 900 °C and milled by attritor (AT) and planetary ball mill (PM), respectively. '(*hkl*)' marks the lattice planes of cubic $Ba_{0.6}Sr_{0.4}TiO_3$ ($d = 3.964$ Å),[10] ♦ corresponds to cubic $(Ba,Sr)F_2$.

Table 3
Results of titration after pyrohydrolysis on calcinated powders and pastes sintered at 1200 °C for 1, 10 and 24 h, respectively.

Sample name	Fluorine content χ[a]			
	Initial powder	1 h	10 h	24 h
P1-AT-· · ·	0.060	0.052	0.017	0.012
P2-AT/PM-· · ·	0.049	0.042	0.017	0.009
P3-PM-· · ·	0.056	0.044	0.019	0.016

[a] Calculated from measured mass fraction, assuming $Ba_{0.6}Sr_{0.4}Ti_{0.99}Co_{0.01}O_{3-\chi}F_\chi$.

80 vol.% particles or aggregates with a diameter above 0.5 μm. For the other powders this value was about 25 vol.% (powder-1-AT) and 40 vol.% (powder-2-PM), respectively. For all powders the remaining volume fraction showed a maximum between 0.05 and 0.10 μm, which is in good agreement with the size of the primary particles seen in the micrographs. Both Laser diffraction and SEM showed that the milling processes were not sufficient to break up the aggregates formed during calcination completely. However, it is assumed that the remaining aggregates were mostly destroyed during paste preparation on the three roll mill, as they could not be seen when checking the pastes with a grindometer.

3.2. Characterization of thick-films

3.2.1. Microstructure

The grain size distribution of the thick-films was determined by image analysis of SEM micrographs taken in top view of the specimen. For each sample 2–5 pictures were analyzed, so that at least 500 grains per thick-film could be evaluated. The counted grains were sorted according to the largest diameter of each grain (i.e. largest distance of two boundary points). Fig. 5 shows evaluated SEM micrographs of each specimen type (3 pastes × 3 sintering times). For better illustration, the grains were partly arranged into different diameter classes and coloured. The pictures clearly show the increasing grain size with sintering time in each row (left → right). In addition, the influence of different powder preparation and powder mixing can be seen by comparing the three rows: As expected from powder characterization, the specimen prepared with the attriton-milled powder (upper row) show the smallest grain diameters, whereas the specimen with planetary ball milled powders (lower row) show the largest ones. The samples with powder mixture (middle row) have a minor amount of small grains beside the large ones and altogether the median grain sizes lie in between the ones of the other samples. Fig. 6 shows the obtained sum curves for all specimen. For further understanding of the influence of grain size on the dielectric properties, the median grain size d_{50} of each specimen was derived from the curves. The values are presented in context with the microwave properties later on (see Table 4).

The height of the thick-films was determined by evaluation of 5 SEM micrographs of breaking edges for each specimen (see also Fig. 5). For the samples sintered for 1 h, the micrographs show a clear boundary between BST and the Al_2O_3 substrate. With increasing sintering time the interface gets less sharp and

Table 4
Characteristic values for the microstructure and the microwave properties of the thick-films prepared with different pastes and sintered for 1 h at 1200 °C, respectively.

Sample name	Microstructure		Microwave properties					
	d_{50} (μm)	P (%)	$\varepsilon_{r,eff}$[a]	$\varepsilon_{r,BST}$[a]	tan δ[a]	tan δ[b]	τ (%)[b]	η[b]
P1-AT-1h	0.26	30.9 ± 3.2	207 ± 11	386 ± 40	0.028 ± 0.002	0.027 ± 0.0002	13.6 ± 0.1	5.01 ± 0.04
P2-AT/PM-1h	0.40	24.6 ± 1.4	260 ± 9	413 ± 20	0.025 ± 0.002	0.026 ± 0.0004	20.0 ± 0.1	7.63 ± 0.11
P3-PM-1h	0.48	31.6 ± 1.3	220 ± 7	419 ± 21	0.019 ± 0.002	0.018 ± 0.0001	22.2 ± 0.2	12.36 ± 0.02

[a] For f = 10 GHz, E = 0 V/μm.
[b] For f = 10 GHz, E = 10 V/μm.

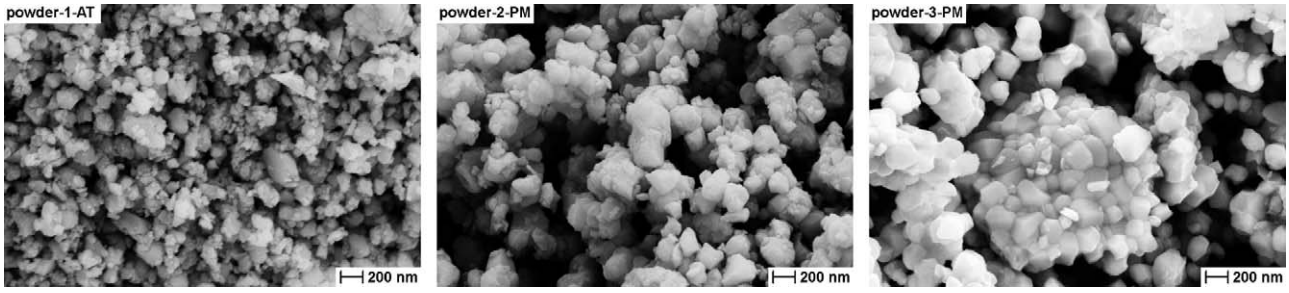

Fig. 4. SEM pictures of the powders calcinated at 900 °C and milled with attritor (AT) and planetary ball mill (PM), respectively.

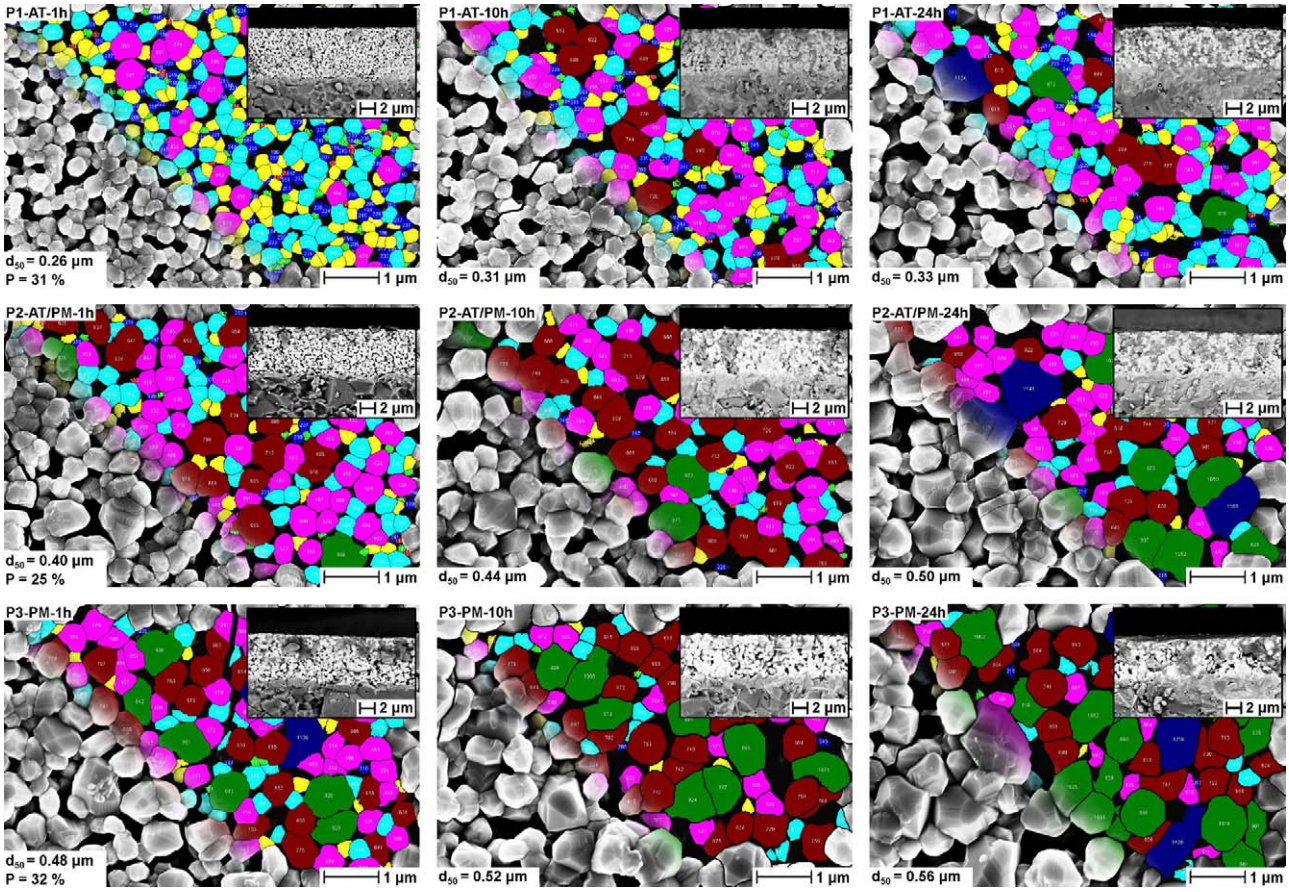

Fig. 5. SEM micrographs of sintered thick-films for different pastes and sintering times (top view and breaking edges). For better illustration of the grain sizes, the pictures were graded and partly coloured. *Gradation:* light red → light green → blue → yellow → turquoise → pink → dark red → dark green → dark blue → purple. (For interpretation of the references to color in this figure legend, the reader is referred to the web version of the article.)

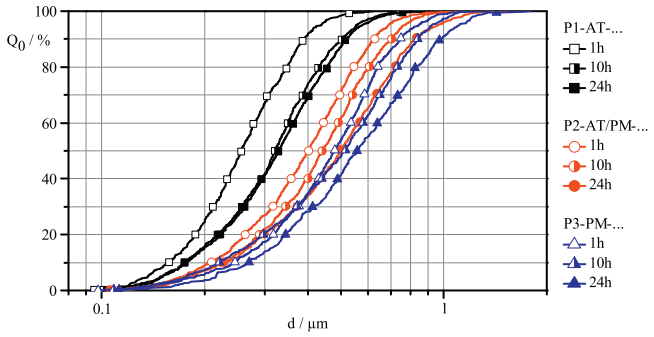

Fig. 6. Sum curves of the grain size distributions of the specimen prepared with 3 different pastes and sintered for 1, 10 and 24 h, respectively.

the BST seems to be smeared into the substrate. This is supposed to be due to the formation of a secondary phase. The diffusion of Ba and Ti in Al_2O_3 and the formation of secondary phases are known from literature.[23–26] Whereas the determined phase composition varies between the publications, all agree that the effect gets severe for temperatures of 1250 °C and higher. With the determined thickness of the films, the porosity of the samples was calculated according to Eq. (2). Specimen P1-AT-1h and P3-PM-1h show porosities of 31% and 32%, respectively, whereas the porosity of P2-AT/PM-1h is 25%. These results are in good agreement with former investigations based on similar paste formulations and sintering conditions.[25] The lower porosity of P2-AT/PM-1h shows the effect of powder mixing on particle packing known from literature.[27,28] For the samples with sintering times above 1 h no reliable determination of porosity was possible due to the formation of the secondary phase and the resulting mass loss of BST.

To further investigate the structure of the thick-films X-ray diffraction measurements were caried out. Fig. 7 shows the patterns of three thick-films prepared with one paste and sintered at different holding times. The graphs illustrate that the predominant phase of all thick-films is cubic BST. In addition to the BST reflexes, all patterns show reflexes of rhomboedric α-Al_2O_3 due to the small thickness of the films (5.5–7 µm). Additionally, a

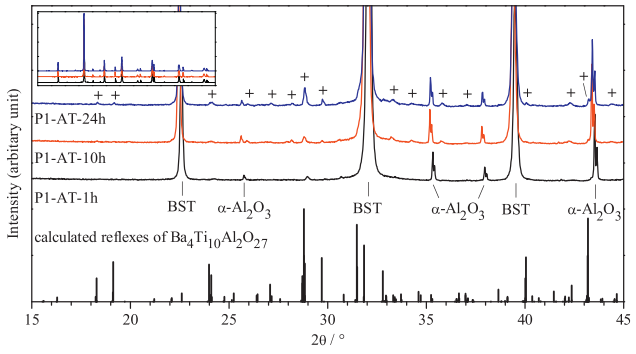

Fig. 7. X-ray diffraction patterns of thick-films sintered at 1200 °C for 1, 10 and 24 h, respectively. The graph in the upper left corner shows an overview ($2\theta = 15° \ldots 80°$) indicating the dominance of the BST phase for all specimen. The main graph shows a section of the patterns (rel. mag. 16×). IN addition to the reflexes of BST and Al_2O_3, the reflexes of one or more undetermined secondary phases are marked (+). In the lower part of the graph calculated reflexes[29,30] of $Ba_4Ti_{10}Al_2O_{27}$ are shown.

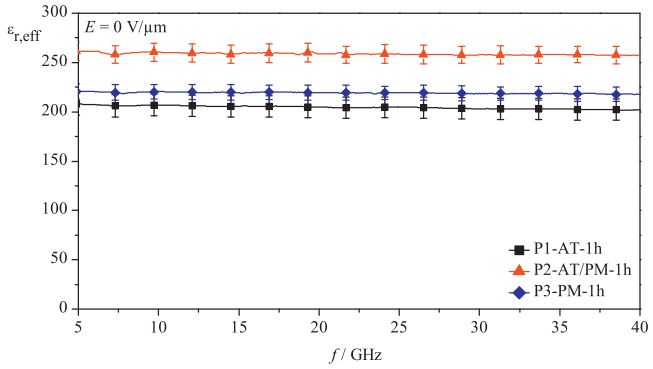

Fig. 8. Relative effective permittivity of the thick-films prepared with different pastes and sintered for 1 h at 1200 °C.

large amount of weak reflexes occurs with increasing sintering time. The strongest of these reflexes was found at $2\theta = 29°$ and can be observed even for the sample sintered for 1 h. Most of the additional reflexes at higher sintering times match the calculated pattern for $Ba_4Ti_{10}Al_2O_{27}$ (ICSD #15272),[29,30] also shown in Fig. 7. However, due to the prescence of Sr, Co, F, possible impurities and the incompleteness of the structure database a definite statement cannot be given at this point. Altogether the X-ray patterns support the results from electron microscopy: For sintering times above 1 h the formation of one or more secondary phases gets severe and probably effects the structure of the remaining BST film.

3.2.2. *Microwave properties*

The dielectric properties of the thick-films were determined by measuring the transmission line characteristics of coplanar waveguides applied on the surface of the specimen. The extraction of permittivity and dielectric loss was done by a conformal mapping method, which considers geometry and properties of the substrate and the waveguides.[19,20] As the dielectric properties of the secondary phase are unknown, a reliable determination of the thick-film properties was only possible for the samples sintered at 1 h. Since the formation of the secondary phase for larger sintering times probably leads to a depletion of one or more elements in the thick-film, a determination of the dielectric properties is not reasonable in this context anyway.

The relative permittivity of the thick-films $\varepsilon_{r,eff}$ in the untuned state ($E = 0$ V/µm) is given in Fig. 8. All thick-films show a permittivity nearly independent on frequency. The values at $f = 10$ GHz are given in Table 4. The specimen with the lowest porosity (P2-AT/PM-1h) shows a significantly higher permittivity compared to the other ones. For the two samples with similar porosities the one with larger grain size (P3-PM-1h) shows larger values for permittivity. To figure out the influence of grain size, the relative permittivity of the material $\varepsilon_{r,BST}$, independent on porosity, was estimated according to Eq. (3) for each sample. The maintained permittivities are given in Table 4. The median values are between 386 and 419 and indicate the increase of permittivity with grain size as discussed above.

The dissipation factor $\tan\delta$ of the thick-films in the untuned state is given in Fig. 9. All three curves show a clear dependency

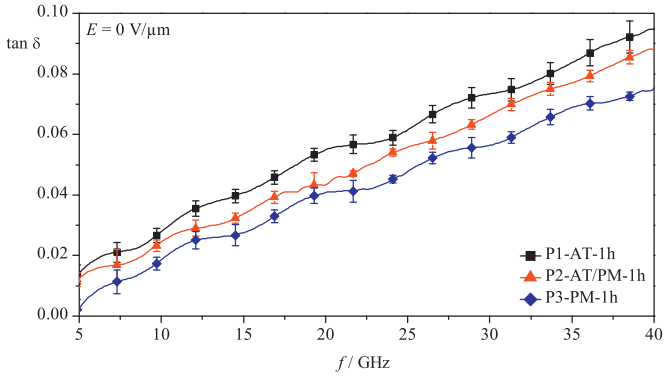

Fig. 9. Dissipation factor of the thick-films prepared with different pastes and sintered for 1 h at 1200 °C.

on frequency, which is known from former investigations.[9,10] Comparing the three curves reveals the influence of microstructure on the dielectric loss: With increasing grain size, the dissipation factor is reduced over the whole frequency range, while an influence of the porosity on the dissipation factor is not noticeable.

The tunability of the thick-films was calculated from the measured permittivity values at $f = 10$ GHz according to Eq. (4). The measured tunability over bias field is shown in Fig. 10.

Assuming a spherical inclusion model, it is predicted by simulation[1,31] for porosities up to $P = 0.2$ that the relative tunability τ of a porous ferroelectric material (tunability of the bulk material: τ_{bulk}) follows the equation:

$$\tau = (1 + 0.2P)\,\tau_{bulk}. \quad (6)$$

This means an increase of tunability with porosity due to local concentrations of the electrical field. However, assuming that this holds also for higher values of P, the dependence on porosity in the studied region is quite weak. Hence the influence of porosity can be neglected, when comparing the measurements of specimens with similar porosities. The measured tunabilities confirm this assumption. Within the considered interval ($0.25 < P < 0.32$) no explicit influence of porosity on tunability can be observed, whereas the influence of grain size is considerable: By increasing the median grain size from 0.26 to 0.48 µm, the tunability at maximum applied bias field ($E = 10$ V/µm) could be raised from about 13.6% (P1-AT-1h) to 22.2% (P3-PM-1h).

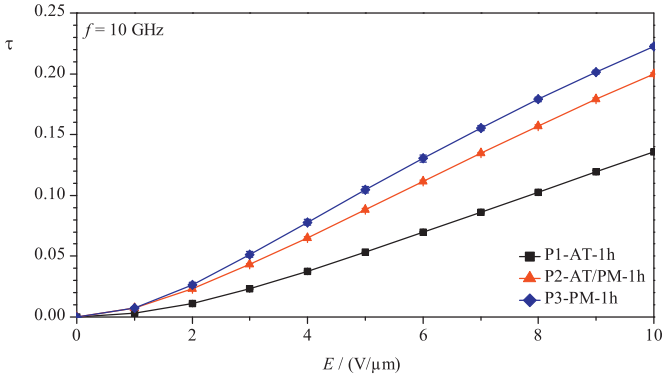

Fig. 10. Tunability of the thick-films prepared with different pastes and sintered for 1 h at 1200 °C.

The material's figure of merit η was calculated according to Eq. 5. For the sample with smallest grain size a value of 5.01 is achieved. As the material's figure of merit is raised with increasing tunability and decreasing dissipation factor, the influence of grain size is quite immense in this case: For specimen P2-AT/PM-1h the median value is 7.63, while specimen P3-PM-1h reaches a value of 12.36.

Table 4 summarizes the results of microstructural investigations and dielectric characterization of the thick-films at microwave frequencies. The values given for the microwave properties are median and standard deviation at a frequency of $f = 10$ GHz.

4. Conclusions

Co–F-codoped $Ba_{0.6}Sr_{0.4}TiO_3$ powders were synthesized through a modified sol–gel process. Powders with different particle sizes were obtained by varying the milling process after calcination of the metal–organic precursor. Screen-printing pastes were prepared and printed on alumina substrates.

Depending on the initial particle size and sintering time a median grain size between 0.26 and 0.56 µm was achieved in the thick-films. For sintering times above 1 h all specimen showed a severe reaction in the interface of the thick-film and the substrate. Hence, no reliable determination of porosity and microwave properties was possible in these cases. For the samples sintered for 1 h the porosity varied between 25% and 31%.

The dielectric characterization at microwave frequencies showed mean values for the relative permittivity of the thick-films between 207 and 260, depending on porosity and grain size. The dissipation factor of the thick-films was reduced for larger grain sizes over the whole frequency range. An influence of the porosity on the dissipation was not noticeable. The thick-films showed no noticeable dependency of tunability on porosity. The influence of grain size however was remarkable. On increasing the grain size from 0.26 to 0.48 µm, the tunability could be raised from 13.6% to 22.2% at maximum applied tuning field.

The investigations show the capability of Co–F-codoped BST thick-films for microwave applications. The achieved dissipation factors lie below the values of other undoped and metal–fluorine-codoped thick-films reported in literature.[10] However, since the fluorine content of the thick-films was higher in this publication and the mechanisms and effects of fluorine doping are not completely understood yet, further investigations have to be carried out. By influencing the thick-film microstructure the tunability of the material was strongly increased while the dissipation factor was even lowered. Hence, in the studied region the best thick-film properties were achieved for the specimen with largest grain size. The determined material's figure of merit was $\eta = 12.36$ in this case.

Acknowledgements

The authors thank Christel Adelhelm (Institute for Applied Materials (IAM-AWP), Karlsruhe Institute of Technology) for the X-ray fluorescence spectroscopy measurements and Florian Stemme (Institute for Applied Materials (IAM-WPT), Karlsruhe Institute of Technology) for the SEM micrographs.

References

1. Tagantsev AK, Sherman VO, Astafiev KF, Venkatesh J, Setter N. Ferroelectric materials for microwave tunable applications. *J Electroceram* 2003;**11**(1–2):5–66.
2. Gevorgian S. *Ferroelectrics in microwave devices, circuits and systems*. 1st ed. London: Springer; 2009.
3. Kong LB, Li S, Zhang TS, Zhai JW, Boey FYC, Ma J. Electrically tunable dielectric materials and strategies to improve their performances. *Prog Mater Sci* 2010;**55**(8):840–93.
4. Herner SB, Selmi FA, Varadan VV, Varadan VK. The effect of various dopants on the dielectric properties of barium strontium titanate. *Mater Lett* 1993;**15**(5–6):317–24.
5. Joshi P, Cole M. Mg-doped $Ba_{0.6}Sr_{0.4}TiO_3$ thin films for tunable microwave applications. *Appl Phys Lett* 2000;**77**(2):289–91.
6. Liang X, Meng Z, Wu W. Effect of acceptor and donor dopants on the dielectric and tunable properties of barium strontium titanate. *J Am Ceram Soc* 2004;**87**(12):2218–22.
7. Zhang Y, Wang G, Chen Y, Cao F, Yang L, Dong X. Effect of donor, acceptor, and donor–acceptor codoping on the electrical properties of $Ba_{0.6}Sr_{0.4}TiO_3$ thin films for tunable device applications. *J Am Ceram Soc* 2009;**92**(11):2759–61.
8. Ye Y, Guo T. Dielectric properties of Fe-doped $Ba_{0.65}Sr_{0.35}TiO_3$ thin films fabricated by the sol–gel method. *Ceram Int* 2009;**35**(7):2761–5.
9. Paul F, Giere A, Menesklou W, Binder JR, Scheele P, Jakoby R, et al. Influence of Fe–F-co-doping on the dielectric properties of $Ba_{0.6}Sr_{0.4}TiO_3$ thick-films. *Int J Mater Res* 2008;**99**(10):1119–28.
10. Zhou X, Gesswein H, Sazegar M, Giere A, Paul F, Jakoby R, et al. Characterization of metal (Fe, Co, Ni, Cu) and fluorine codoped barium strontium titanate thick-films for microwave applications. *J Electroceram* 2010;**24**(4):345–54.
11. Ihrig H. The phase stability of $BaTiO_3$ as a function of doped 3d elements: an experimental study. *J Phys C: Solid State* 1978;**11**(4):819–27.
12. Hagemann HJ, Ihrig H. Valence change and phase stability of 3*d*-doped $BaTiO_3$ annealed in oxygen and hydrogen. *Phys Rev B* 1979;**20**(9): 3871–8.
13. Arlt G, Hennings D, de With G. Dielectric properties of fine-grained barium titanate ceramics. *J Appl Phys* 1985;**58**(4):1619–25.
14. Arlt G. The influence of microstructure on the properties of ferroelectric ceramics. *Ferroelectrics* 1990;**104**(1):217–27.
15. Zhang L, Zhong L, Wang CL, Zhang PL, Wang YG. Dielectric properties of $Ba_{0.7}Sr_{0.3}TiO_3$ ceramics with different grain size. *Phys Status Solidi A* 1998;**168**(2):542–8.
16. Zhang L, Zhong WL, Wang CL, Zhang PL, Wang YG. Finite-size effects in ferroelectric solid solution $Ba_xSr_{1-x}TiO_3$. *J Phys D: Appl Phys* 1999;**32**(5):546–51.
17. Giere A, Zhou X, Paul F, Sazegar M, Zheng Y, Maune H, et al. Barium strontium titanate thick-films: dependency between dielectric performance and their morphology. *Frequenz* 2008;**62**(3–4):47–51.
18. Wilhoit R, Zwolinski B. Physical and thermodynamis properties of aliphatic alcohols. *J Phys Chem Ref Data* 1973;**2**(1):1–420.
19. Carlsson E, Gevorgian S. Conformal mapping of the field and charge distributions in multilayered substrate CPW's. *IEEE Trans Microw Theory* 1999;**47**(8):1544–52.
20. Ouaddari M, Delprat S, Vidal F, Chaker M, Wu K. Microwave characterization of ferroelectric thin-film materials. *IEEE Trans Microw Theory* 2005;**53**(4):1390–7.
21. Wersing W, Lubitz K, Mohaupt J. Dielectric, elastic and piezoelectric properties of porous pzt ceramics. *Ferroelectrics* 1986;**68**(1):77–97.
22. Auciello O, Saha S, Kaufman D, Streiffer S, Fan W, Kabius B, et al. Science and technology of high dielectric constant thin films and materials integration for application to high frequency devices. *J Electroceram* 2004;**12**(1-2):119–31.
23. Sengupta LC, Stowell S, Ngo E, O'Day M, Lancto R. Barium strontium titanate and non-ferroelectric oxide ceramic composites for use in phased array antennas. *Integr Ferroelectr* 1995;**8**(1–2):77–88.
24. Su B, Button T. Interactions between barium strontium titanate (BST) thick films and alumina substrates. *J Eur Ceram Soc* 2001;**21**:2777–81.
25. Paul F, Binder JR, Berto A, Link G, Ritzhaupt-Kleissl HJ. Influence of the process parameters on the microstructure of screen-printed $Ba_{0.6}Sr_{0.4}TiO_3$ (BST60) thick-films on alumina-substrates. In: Menz W, Dimov S, Fillon B, editors. *4M 2006 – second international conference on multi-material micro manufacture*. Oxford: Elsevier; 2006. p. 221–9.
26. Jiansirisomboon S, Watcharapasorn A, Tunkasiri T. Effects of Al_2O_3 nano-particulates addition on barium titanate ceramics. *Chiang Mai J Sci* 2006;**33**(2):175–82.
27. McGeary RK. Mechanical packing of spherical particles. *J Am Ceram Soc* 1961;**44**(10):513–22.
28. Cumberland DJ, Crawford RJ. *The packing of particles*. Amsterdam: Elsevier; 1987.
29. Schmachtel J, Müller-Buschbaum H. Ein neues quaternäres Oxotitanat: $Ba_4Ti_{10}Al_2O_{27}$. *Z Anorg Allg Chem* 1981;**472**(1):89–94.
30. NIST FK. *Inorganiccrystalstructuredatabase*(*ICSD*); 2010.
31. Sherman V, Tagantsev A, Setter N. Tunability and loss of the ferroelectric–dielectric composites. In: *14th IEEE international symposium on applications of ferroelectrics*. 2004. p. 33–8.